Near-Field Electromagnetic Theory for Thin Solar Cells

A. Niv,[1] M. Gharghi,[1] C. Gladden,[1] O. D. Miller,[2,3] and X. Zhang[1,3,*]

[1]*NSF Nanoscale Science and Engineering Center (NSEC), University of California, Berkeley, California 94720, USA*
[2]*Electrical Engineering & Computer Sciences Department, University of California, Berkeley, California 94720, USA*
[3]*Materials Science Division, Lawrence Berkeley National Laboratory, Berkeley, California 94720, USA*

Current methods for evaluating solar cell efficiencies cannot be applied to low-dimensional structures where phenomena from the realm of near-field optics prevail. We present a theoretical approach to analyze solar cell performance by allowing rigorous electromagnetic calculations of the emission rate using the fluctuation-dissipation theorem. Our approach shows the direct quantification of the voltage, current, and efficiency of low-dimensional solar cells. This approach is demonstrated by calculating the voltage and the efficiency of a GaAs slab solar cell for thicknesses from several microns down to a few nanometers. This example highlights the ability of the proposed approach to capture the role of optical near-field effects in solar cell performance.

In view of the demand for more efficient solar energy conversion at lower cost, low-dimensional solar cell geometries such as nanostructured and ultrathin devices are needed to decrease material usage, enhance light-matter interaction, and allow more efficient charge collection. With the reduced optical thickness of the absorber material in such cells, electromagnetic phenomena such as propagating surface plasmons, nano-optic cavities, and photonic crystals have been pursued to enhance the absorption [1–8], which in turn translates to higher photocurrent. While these optical near-field mechanisms are generally considered as a means to enhance the current (I), a successful solar cell must maximize the output power, which is the current-voltage product $I \times V$, rather than the current alone. This power is obtained from the I-V relation $I = I_{ph} - I_{rec}(V)$. The photocurrent $I_{ph} = q \times R_{in}$ is determined by the absorbed solar photon flux R_{in}, as depicted in Fig. 1, where q is the electronic charge. The recombination current I_{rec} is a function of the voltage V and reduces to the saturation current of the cell at $V = 0$. In the absence of nonradiative processes, which is commonly considered for the theoretical efficiency prediction of solar cells [9,10], I_{rec} is related to the photon flux R_{out} emitted by the solar cell ($I_{rec} = q \times R_{out}$). Traditionally, theories predicting cell efficiencies are based on a ray optics analysis of R_{out} [9–14]. Near-field electromagnetic phenomena, however, can have dramatic effects on the behavior of solar cells when structural dimensions are far below the typical wavelength of solar light. While calculating the absorption R_{in} in the presence of such phenomena has been widely studied using concepts such as the local density of states [15–19], no equivalent framework yet exists for the emission rate R_{out} [20].

Here, an analysis of solar cell performance that is based on the electromagnetic nature of the spontaneous emission rate R_{out} is presented. This is obtained by exploiting the

fluctuation-dissipation theorem [21–25] to relate the thermodynamic properties of the cell with sources of electromagnetic radiation, such as charge dipoles. The given analysis enables for the first time quantification of the voltage, current, and efficiency of low-dimensional structures in the presence of optical near-field effects. First, the spontaneous emission rate from a given body of material is developed based on macroscopic-electromagnetics and irreversible-thermodynamics principles. The theory is followed by application of the new formalism to a simple model of a slab solar cell. Although not a practical device by itself, structural simplicity of the chosen cell allows a
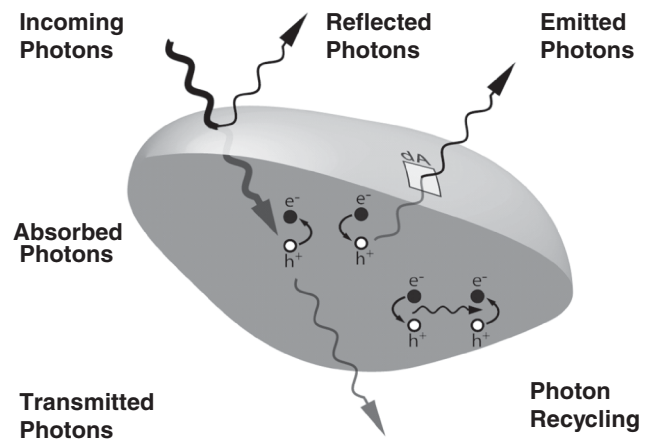

FIG. 1. Optical processes in a semiconductor. The absorbed fraction of incoming photons excites electron-hole pairs leading to the cell photocurrent. The emission from recombination of these excited states can be considered as the electromagnetic power leaving the cell surface. Not all radiative recombinations contribute to the emission; some are recycled. The population of the excited electrons establishes the (chemical) potential throughout the material volume.

clear demonstration of the ability of our new approach in capturing the electromagnetic aspects of spontaneous emission, including near-field effects.

The emission rate R_{out} from a given body of material (see Fig. 1) can be obtained from dividing the power flux emanating from its surface A by the photon energy $\hbar\omega$ ($\hbar$ is the reduced Plank constant, ω is the temporal angular frequency) [26]:

$$R_{out} = \int_A dA \int_0^\infty \frac{d\omega}{\hbar\omega} \langle \mathbf{S}(\mathbf{r}, \omega) \rangle \cdot \hat{\mathbf{n}}, \qquad (1)$$

where $\hat{\mathbf{n}}$ and $\mathbf{r}$ are the surface normal and the surface position vectors, and $\langle \mathbf{S}(\mathbf{r}, \omega) \rangle = \frac{1}{2} \langle \mathbf{E} \times \mathbf{H}^* \rangle$ is the spectral representation of the ensemble-averaged Poynting vector, where $\mathbf{E}$ and $\mathbf{H}$ are the electric and magnetic fields, respectively. The $\mathbf{E}$ and $\mathbf{H}$ fields, at each location on the surface, relate to the volume density of radiating dipoles by the respective Green dyads e_{jm} and h_{lk}. Using this tensor notation, we can formally write

$$\langle S_i(\mathbf{r}, \omega) \rangle = \frac{1}{2} \iint_{\tilde{V}} dr_1^3 dr_2^3 \varepsilon_{ijk} e_{jm}(\mathbf{r} - \mathbf{r}_1)$$
$$\times P_{ml}(\mathbf{r}_1, \mathbf{r}_2, \omega) h_{lk}^*(\mathbf{r} - \mathbf{r}_2) + \text{c.c.}, \quad (2)$$

where $P_{ml}(\mathbf{r}_1, \mathbf{r}_2, \omega) = \langle p_m(\mathbf{r}_1) p_l^*(\mathbf{r}_2) \rangle_\omega$ is the statistical ensemble-averaged correlation dyad of dipole densities at locations $\mathbf{r}_1$ and $\mathbf{r}_2$, and polarization m and l, at frequency ω [24,25]. As usual in tensor notation, ε_{ijk} is the Levi-Civita tensor; $i, j, k, m,$ and l run over the three possible electric or magnetic field polarizations, and summation over repeated indices is assumed. In addition, the $*$ sign as well as the c.c. denote complex conjugation. The electric and magnetic Green dyads can be analytically evaluated for every configuration with a known (discrete or continuous) electromagnetic modal structure [27] or alternatively be numerically evaluated for an arbitrary given structure [28].

At this stage, the correlations of radiating dipoles $P_{ml}(\mathbf{r}_1, \mathbf{r}_2, \omega)$ are considered as spontaneous fluctuations of a stationary canonical linear system, locally at a state of equilibrium. Statistical mechanics allows us to connect the relaxation of a nonequilibrium state with these spontaneous microscopic dynamics of the equilibrium system [24]—a connection known as the fluctuation-dissipation theorem [22]:

$$P_{ml}(\mathbf{r}_1, \mathbf{r}_2; \omega) = \frac{\hbar\omega}{2} \coth(\hbar\omega/2k_B T_0) \phi_{ml}(\mathbf{r}_1, \mathbf{r}_2; \omega), \quad (3)$$

where ϕ_{ml} is the systems dissipation function at temperature T_0 and k_B is Boltzmann's constant. The given formalism establishes a connection between local dissipation events at the interior of the material volume and the photon emission from its surface. In Eq. (3), the process of radiative recombination (and emission of a photon) in a semiconducting material is represented by a canonical ensemble of dipole densities acting as sources of electromagnetic fields. The power emitted from these sources to the surroundings at a specific surface location and frequency is calculated in Eq. (2). Finally, Eq. (1) integrates over surface and frequency to give the total emission rate from the material body.

In order to have a meaningful formalism, the correct dissipation function ϕ_{ml} must be identified. This can be obtained by acknowledging that the formalism must eventually obey the known macroscopic behavior of semiconductors. Consequently, the dissipation of spontaneous (ϕ_{Spont}) and stimulated (ϕ_{Stim}) transitions between the valance and the conduction bands of the semiconductor are considered. At thermal equilibrium, the following relation must hold [29]:

$$\phi_{Spont}/\phi_{Stim} = \{\exp[(E - \Delta F)/k_B T_0] - 1\}^{-1}. \quad (4)$$

$E = \hbar\omega$, and $\Delta F = F_n - F_p = qV$ is the separation of quasi-Fermi levels of electrons (F_n) and holes (F_p). The stimulated dissipation ϕ_{Stim} is proportional to the net electromagnetic loss in the material [29,30]. According to the electromagnetic energy theorem of nonmagnetic materials, this loss is associated with the imaginary part of the material permittivity [31]. Consequently, $\phi_{Stim} = \varepsilon''$ and the electromagnetic dissipation function for a material at temp T_0 and potential V transpires:

$$\phi_{ij}(\mathbf{r}_1, \mathbf{r}_2; \omega) = \frac{\varepsilon''(\mathbf{r}_2, \omega)}{\exp[(\hbar\omega - qV)/k_B T_0] - 1} \delta(\mathbf{r}_1 - \mathbf{r}_2) \delta_{ij}. \quad (5)$$

The Dirac and Kronecker delta functions express the local character of the fluctuations and the orthogonality of the electric field polarization, respectively. The above formula reduces to the known expression of the fluctuation-dissipation theorem in nonsemiconducting materials once $V = 0$ [23,25] and leads to the well-known expression for thermal emission from an infinite semiconductor [32].

Equations (1)–(3) together with the dissipation function of Eq. (5) establish a rigorous electromagnetic approach for the characterization of spontaneous emission from a solar cell (and in fact any body of material) at temperature T_0 and potential V. The semiconductor band gap is introduced into this formalism naturally by the material complex permittivity $\varepsilon = \varepsilon' + i\varepsilon''$, and therefore the integration in Eq. (1) starts from zero rather than from the band gap frequency. Commonly, the concept of density of states is invoked to express electromagnetic effects on the event of dissipation [6,16–19]. However, the density of states can only express the local effect of the electromagnetic environment on the internal event of radiative recombinations, while the present formalism accounts for the surface emission from such a process. It is this surface emission, and not the internal processes, that establishes a thermodynamic balance to the absorbed solar flux [9–14]. As such, this formalism provides an effective methodology to assess and optimize the performance of low-dimensional
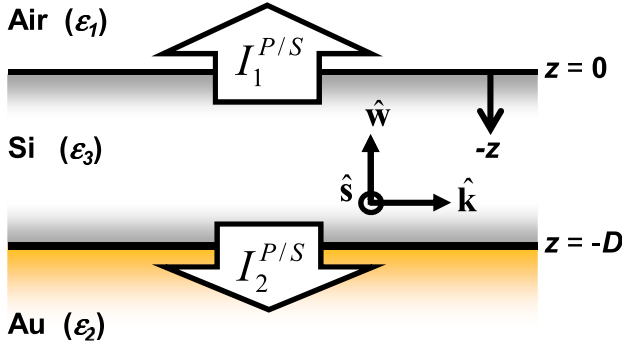
FIG. 2 (color online). Schematic layout of a slab GaAs solar cell with a metallic gold (Au) back reflector. Block arrows represent the four possible emission channels: GaAs to air—$I^{P/S}_1$ and GaAs to Au substrate—$I^{P/S}_2$, for S (TE) and P (TM) polarizations.

solar cells by accounting for optical near-field effects. The system under consideration is assumed to be characterized by the single spatially invariant potential V. This assumption is common for semiconductor solar cells [9,10] and

becomes more justified once reduced dimensions, much smaller than the carrier diffusion length, are considered.

To demonstrate an example application of the presented approach, let us consider a solar cell consisting of a thin GaAs (band gap 1.42 eV) slab and a gold back reflector, as depicted in Fig. 2. This device lacks the level of sophistication of a practical solar cell, yet its structural simplicity allows analytic evaluation of the cell performance. When scaled to small thicknesses, near-field optical effects are expected to influence the rate of emission and therefore the performance of this cell. Since spontaneous radiative recombinations and their eventual emission are of interest, all charge transport and separation mechanisms are trivially considered to be perfect. Direct insertion of the Green dyads of this structure, as derived by Sipe [33], into Eq. (2) gives a closed-form formula for the emission rate from the device, as a function of cell thickness [32]. Four possible emission channels $I^{S/P}_{1/2}$ exist in this case, for the electromagnetic power flow with perpendicular (S) and parallel (P) polarization and through the two interfaces (1, air/GaAs; 2, GaAs/Au):
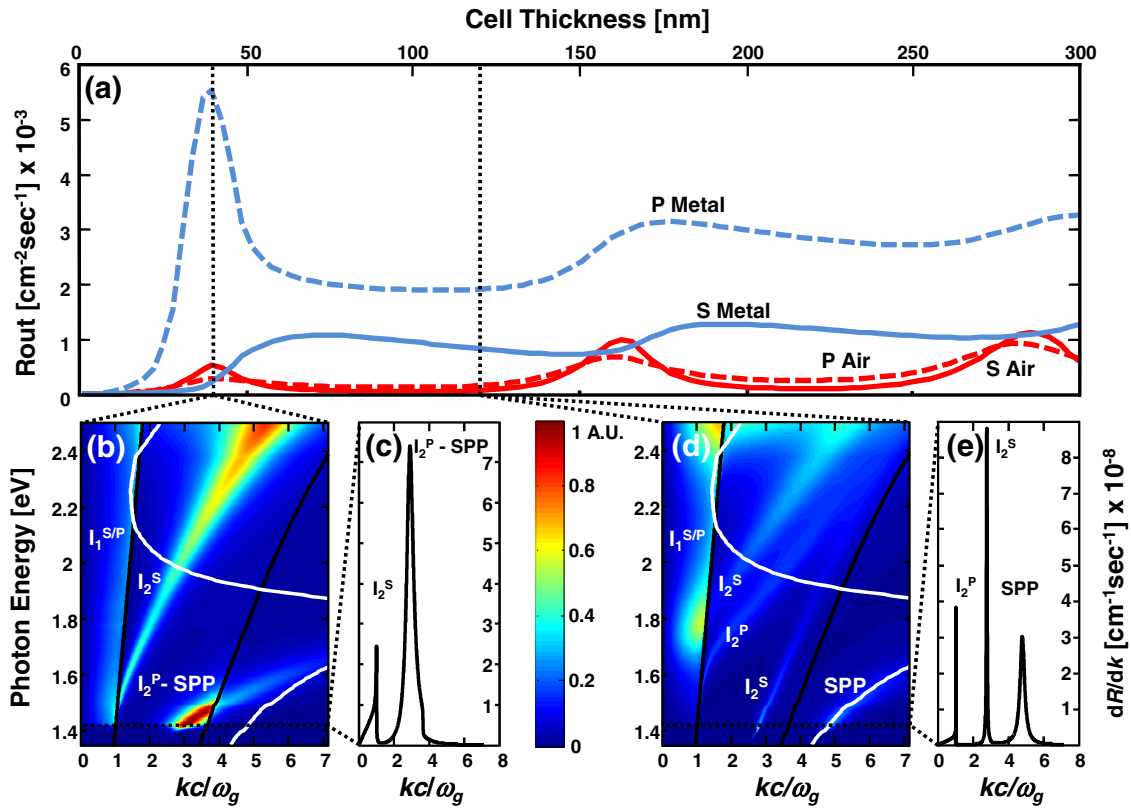

FIG. 3 (color online).   (a) Emission rate (R_{out}) of the S and P polarizations through GaAs/air and GaAs/Au interfaces as a function of cell thickness. Panels (b) and (d) show emission intensity maps at 40 and 120 nm thicknesses, respectively. Black lines represent the analytic dispersion of plane waves in air (to the left) and in GaAs (to the right), while white lines depict the analytical single-sided SPP dispersion at the GaAs/Au interface. At 120 nm thickness (d), the emission clearly occurs into guided modes above and below the light line ($I^{S/P}_{1/2}$) and separately into the single-sided SPP mode. At 40 nm (b), the surface plasmon mode interacts with the second interface, resulting in a hybrid I^P_2 SPP mode that is guided at higher energies. Panels (c) and (e) show emission vs normalized wave number at 1.42 eV (the GaAs band gap) for the two thicknesses, respectively. All results are derived for $V = 0$ and $T_0 = 300°$ K.

$$R_{\text{out}} = \frac{1}{4\pi^3} \exp\left(\frac{qV}{k_B T_0}\right) \int_0^\infty d\omega \exp\left(\frac{-\hbar\omega}{k_B T_0}\right)$$
$$\times \int_0^\infty k\,dk (I_1^S + I_1^P + I_2^S + I_2^P). \quad (6)$$

Figure 3(a) shows the individual contributions of emission rates as a function of GaAs slab thickness for $V = 0$ and $T_0 = 300°$ K. The sum of these four comprises the total emission rate out of the cell. As opposed to a ray optical model, all the electromagnetic aspects of the emission process are captured by the current formalism. These include the cavitylike resonance between the (partially) reflective interfaces responsible for the oscillations in the emission rates, as well as optical near-field effects. A clear signature of such a near-field effect is the anomalous peak in the P-polarization emission into the metal, at 40 nm thickness.

For a detailed investigation of this near-field phenomenon, we set our attention on two GaAs slab thicknesses of 40 and 120 nm. Figures 3(b) and 3(d) depict intensity maps of the total emission rate as a function of wave number (normalized to ω_g/c) and photon energy. Regions of intense emission are labeled according to the dominant channel. Black lines represent the analytic dispersion of plane waves in air and GaAs. These lines divide the emission maps into three distinct regions: the region dominated by waves propagating in air to the left, guided modes propagating in GaAs with an evanescent tail in air in the middle, and waves evanescent in both air and GaAs to the right. For both thicknesses, the emission into air (I_1^S and I_1^P) is confined to the leftmost region. At 120 nm thickness [Fig. 3(d)], the emission occurs into clearly divisible guided and surface plasmon-polariton (SPP) modes. Close to the band gap energy, where the emission is most intense, through the Boltzmann factor in Eq. (6), none of the modes reveals strong emission from the air or metal interfaces. Accordingly, the cross section plot at 1.42 eV photon energy [Fig. 3(e)] reveals a relatively weak emission from the SPP mode. At 40 nm, on the other hand [Fig. 3(b)], the close proximity of the second interface shifts the SPP mode to higher energies, resulting in a hybrid I_2^P SPP mode that is guided in the GaAs for $E \leq \sim 1.5$ eV and SPP-like for $E > \sim 1.5$ eV. As shown in Fig. 3(c), this mode strongly couples the GaAs band gap radiative recombination to the P-polarized emission peak through the metal interface. This is indeed the optical near-field effect responsible for the anomalous emission peak at 40 nm of Fig. 3(a). The above discussion shows the ability of our approach in capturing the physical mechanisms underlying radiative emission from a solar cell, including optical near-field effects.

Finally, the cell performance is established from the detailed balance between emission and absorption rates. Absorption is calculated from the assumed solar flux considered as a blackbody radiation at a temperature

$T_s = 5800°$ K, integrated from the band gap frequency (ω_g) and above, that is included in the solid angle subtended by the Sun $\Omega_S = 6.85 \times 10^{-5}$ sr:

$$R_{\text{in}} = \frac{\Omega_S}{4\pi^3 c^2} \int_{\omega_g}^\infty \frac{\sigma(\omega)\omega^2 d\omega}{\exp(\hbar\omega/k_B T_S) - 1}, \quad (7)$$

where c is the speed of light. The absorbance of the cell $\sigma(\omega)$ depends on the semiconductor absorption coefficient and the structure geometry and can be obtained from exact transmission matrix formalism for the reflection and transmission at the interfaces of the layered geometry [34]. While revealing an interference signature due to multiple reflections from the front and back interfaces, R_{in} will not show any of the guided or SPP near-field modes characteristic to R_{out} in this device. The reason is that the solar flux is considered as radiation coming from a source at infinity.

The I-V curve of the device is derived from $I(V) = q[R_{\text{in}} - R_{\text{out}}(V)]$. Open circuit voltage V_{oc} is obtained at zero current $I(V_{\text{oc}}) = 0$, and efficiency is found by maximizing the $I \times V$ product. Figure 4 shows the open circuit voltage as a function of cell thickness for the GaAs device. For comparison, the dashed red line shows the V_{oc} of the ray-based formalisms [12]. The ray-based model fails to predict the V_{oc} for small GaAs slab thicknesses as it does not account for the electromagnetic nature of the emission, including near-field effects. One such near-field effect is the P-polarization emission peak at 40 nm thickness discussed earlier, which is responsible for the dip in V_{oc} observed at this thickness. The voltage is affected by the electromagnetic phenomena that govern both emission and absorption processes at each thickness. Therefore, the oscillations in V_{oc} are somewhat displaced with respect to those of Fig. 3(a) and fade away in thicker cells due to GaAs absorption. Comparing our predicted values with the ray-based model for small GaAs slab thicknesses shows
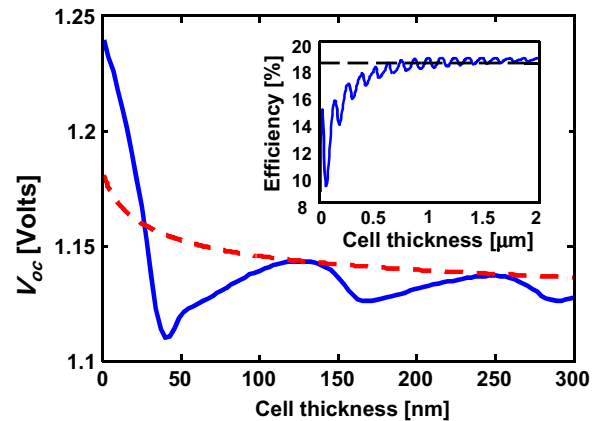

FIG. 4 (color online). Open circuit voltage vs cell thickness of our formalism (solid blue line) compared to a ray-based model (dashed red line). Oscillations result from both absorption and emission and tend to relax for thick cells due to GaAs absorption. The inset shows efficiency vs cell thickness.

that considerations beyond merely absorption enhancement [1–8] must be taken into account for the design of future ultrathin devices.

The inset of Fig. 4 shows the efficiency of the GaAs slab cell. The asymptotic efficiency of 18.4% (and V_{oc} of 1.12 V) for a very thick GaAs solar cell without an antireflection coating is in agreement with ray optics based models [12]. We also note that, in spite of the voltage rise, the efficiency for an extremely thin slab eventually drops due to diminishing absorption in this device and thus to a vanishing photocurrent. Therefore, while capturing the electromagnetic nature of the photovoltage and photocurrent production in thin solar cells, our analysis converges to the known and expected results in the asymptotic limits of thick and thin devices.

In conclusion, we have applied the fluctuation-dissipation theorem to connect the thermodynamic and the electromagnetic aspects of spontaneous emission from a semiconducting material. This gives a rigorous electromagnetic framework for evaluating solar cell performance under conditions unattainable by previous approaches, i.e., the optical near-field regime. This analysis accounts for all optical aspects of power generation in solar cells, including optical losses and dispersion. While the theory targets only radiative recombination, the effect of nonradiative losses can be incorporated by a voltage dependent luminescence quantum yield, similar to other theoretical cell efficiency schemes [11,12]. The analysis was demonstrated for a simplified model of a solar cell, indicating that near-field effects may eventually suppress emission rather than only increasing the absorption—a fact that may benefit future cell designs. Characterization of a viable design may follow similar steps, albeit with a numerical evaluation of the Green dyads for the more sophisticated structure. Finally, this analysis is not limited to semiconductors and can be applied to any system within the macroscopic view of Maxwell equations.

*To whom all correspondence should be addressed.
xiang@berkeley.edu

[1] H. R. Stuart and D. G. Hall, J. Opt. Soc. Am. A **14**, 3001 (1997).

[2] H. R. Stuart and D. G. Hall, Phys. Rev. Lett. **80**, 5663 (1998).

[3] D. M. Schaadt, B. Feng, and E. T. Yu, Appl. Phys. Lett. **86**, 063106 (2005).

[4] D. Derkacs, S. H. Lim, P. Matheu, W. Mar, and E. T. Yu, Appl. Phys. Lett. **89**, 093103 (2006).

[5] S. Pillai, K. R. Catchpole, T. Trupke, and M. A. Green, J. Appl. Phys. **101**, 093105 (2007).

[6] K. R. Catchpole and A. Polman, Opt. Express **16**, 21 793 (2008).

[7] V. E. Ferry, L. A. Sweatlock, D. P. Pacifici, and H. A. Atwater, Nano Lett. **8**, 4391 (2008).

[8] H. A. Atwater and A. Polman, Nature Mater. **9**, 205 (2010).

[9] W. Shockley and H. J. Queisser, J. Appl. Phys. **32**, 510 (1961).

[10] W. Ruppel and P. Würfel, IEEE Trans. Electron Devices **27**, 877 (1980).

[11] R. T. Ross, J. Chem. Phys. **46**, 4590 (1967).

[12] T. T. Tiedje, E. Yablonovitch, G. D. Cody, and B. G. Brooks, IEEE Trans. Electron Devices **31**, 711 (1984).

[13] T. Markvart, Appl. Phys. Lett. **91**, 064102 (2007).

[14] M. Green, *Solar Cells* (Prentice-Hall, Englewood Cliffs, NJ, 1998).

[15] P. Sheng, A. N. Bloch, and R. S. Stepleman, Appl. Phys. Lett. **43**, 579 (1983).

[16] P. N. Saeta, V. E. Ferry, D. Pacifici, J. N. Munday, and H. A. Atwater, Opt. Express **17**, 20 975 (2009).

[17] Z. F. Yu, A. Raman, and S. H. Fan, Proc. Natl. Acad. Sci. U.S.A. **107**, 17 491 (2010).

[18] E. A. Schiff, J. Appl. Phys. **110**, 104501 (2011).

[19] D. M. Callahan, J. N. Munday, and H. A. Atwater, Nano Lett. **12**, 214 (2012).

[20] The use of electromagnetic reciprocity relations is not practical in this case since the absorption from a remote source is not exposed to the near-field environment available to the emission process.

[21] H. B. Callen and T. A. Welton, Phys. Rev. **83**, 34 (1951).

[22] R. Kubo, M. Toda, and N. Hashitsume, *Statistical Physics II* (Springer-Verlag, Berlin, 1995), 2nd ed.

[23] D. Polder and M. Van Hove, Phys. Rev. B **4**, 3303 (1971).

[24] D. Chandler, *Introduction to Modern Statistical Mechanics* (Oxford University Press, Oxford, England, 1987).

[25] W. Eckhardt, Opt. Commun. **41**, 305 (1982).

[26] All units are in the electromagnetic variant of the centimeter-gram-second system (EMU CGS), except for those of voltage (V) and current (I), which are in the International System of Units (SI).

[27] E. Economou, *Green's Functions in Quantum Physics* (Springer, Berlin, 1983), 3rd ed.

[28] A. J. Ward and J. B. Pendry, Phys. Rev. B **58**, 7252 (1998).

[29] G. Lasher and F. Stern, Phys. Rev. **133**, A553 (1964).

[30] P. K. Basu, *Theory of Optical Processes in Semiconductors* (Oxford University Press, Oxford, England, 1997).

[31] L. D. Landau and E. M. Lifshitz, *Electromagnetics of Continuous Media* (Elsevier, New York, 2004), 2nd ed.

[32] See Supplemental Material at http://link.aps.org/supplemental/10.1103/PhysRevLett.109.138701 for a detailed derivation of the reported results.

[33] J. E. Sipe, J. Opt. Soc. Am. B **4**, 481 (1987).

[34] M. Born and E. Wolf, *Principles of Optics* (Cambridge University Press, New York, 1999), 7th ed.